Available online at www.sciencedirect.com
ScienceDirect
Polymer 49 (2008) 1659–1675
polymer
www.elsevier.com/locate/polymer

Gas transport properties of MgO filled poly(1-trimethylsilyl-1-propyne) nanocomposites

Scott Matteucci, Victor A. Kusuma, Scott D. Kelman, Benny D. Freeman*

Department of Chemical Engineering, The University of Texas at Austin, 10100 Burnet Road, Building 133, Austin, TX 78758, USA

Received 5 October 2007; received in revised form 22 December 2007; accepted 5 January 2008
Available online 11 January 2008

Abstract

Magnesium oxide (MgO) nanoparticles were dispersed via solution processing in poly(1-trimethylsilyl-1-propyne) (PTMSP) to form polymer nanocomposites. Transmission electron microscopy was used to determine the extent of particle aggregation in the composites. Both nanocomposite density and CO_2, CH_4, N_2, and H_2 permeability were influenced by nanoparticle loading. Nanocomposite densities were markedly lower than predicted by a two phase additive model. For example, in films containing 75 nominal volume percent MgO, the polymer–particle composite density was 68 percent lower than expected based on an additive model. At this loading, gas permeability coefficients were, depending on the gas, 17–50 times higher than in unfilled PTMSP at similar conditions. The changes in permeability with particle content were interpreted in terms of measured changes in gas solubility with particle content and diffusion coefficients calculated from the permeability and solubility data.

Keywords: Nanocomposite; Membrane; MgO

1. Introduction

Heterogeneous materials comprising a polymer matrix and an inorganic dispersed phase have recently attracted interest as a platform to potentially prepare improved gas separation membranes [1–5]. Polymers can be processed into defect-free, large surface area, thin membranes that withstand high pressures and exhibit significant gas flux and selectivity [6]. However, there is a limit, called the ''upper bound'', to the levels of permeability and selectivity that can be achieved with polymers alone [7,8]. It has been suggested that inorganic fillers (*e.g.*, zeolites or impermeable particles) may alter light gas transport properties when they are dispersed in a polymer matrix in such a way that the gas transport properties of the resulting composite materials exceed the properties that can be obtained with polymers alone [3,4,9–14].

Traditionally, transport properties in polymer/inorganic heterophase materials exhibit permeability behavior reflecting the transport properties of the individual phases [9–11]. For example, dispersing 6 volume percent graphite (*i.e.*, an impermeable particle) into poly(dimethylsiloxane) resulted in N_2 permeability values that were 34 percent lower than that in the unfilled polymer [15]. However, exceptions to such behavior are known. For example, He et al. reported an increase in gas permeability as the concentration of fine particles (*i.e.*, 13 nm primary particle diameter fumed silica (FS)) increased in high free volume, rigid polymers [12]. Specifically, poly(4-methyl-2-pentyne) (PMP) filled with 25 volume percent FS exhibited N_2 permeability coefficients approximately 3 times higher than that of unfilled PMP [12]. FS particles did not alter gas solubility much in the nanocomposites, but the particles did significantly increase gas diffusion coefficients [13]. For example, CH_4 diffusion coefficients doubled in PMP containing 30 wt.% FS [13]. The FS particles were sufficiently small that they could disrupt chain packing in the glassy, stiff-chain, high free volume polymers, which increased fractional free volume, as demonstrated by positron annihilation lifetime spectroscopy [2]. Increasing fractional free volume caused gas diffusion coefficients to increase, which, in turn, increased gas permeability [16].

* Corresponding author. Tel.: +1 512 232 2803; fax: +1 512 232 2807.
E-mail address: freeman@che.utexas.edu (B.D. Freeman).

0032-3861/$ - see front matter © 2008 Elsevier Ltd. All rights reserved.
doi:10.1016/j.polymer.2008.01.004

In addition to using particles to influence gas diffusivity in polymer-based composites, nanoparticles incorporated into polymers can alter their solubility towards a specific penetrant gas [3,17]. For instance, propylene/propane selectivity increased from near unity in a poly(ethylene-*co*-propylene) film to ~180 in a poly(ethylene-*co*-propylene) film containing 50 wt.% Ag nanoparticles and 0.8 wt.% *p*-benzoquinone [17]. The increase in selectivity was attributed to the affinity of propylene for the silver nanoparticles, which presumably increased propylene/propane solubility selectivity in the nanocomposites. Some particles exhibit much higher gas solubility than polymers. For example, Paul and Kemp added micron-sized zeolite particles to silicon rubber [18]. The zeolite adsorbed 140 cm^3(STP) CO_2/cm^3 of particles at 1 atm, while the polymer sorbed only 1.1 cm^3(STP)/cm^3 of polymer of CO_2 at 1 atm [18]. Based on their studies, such fillers had very little effect on steady-state gas transport properties because CO_2 adsorbed so strongly to the zeolites that it could not be easily desorbed during typical steady-state permeation experiments [18].

This study reports the influence of impermeable periclase (*i.e.*, MgO) nanoparticles on pure gas permeability coefficients in poly(1-trimethylsilyl-1-propyne) (PTMSP) based nanocomposites. The MgO/PTMSP nanocomposites exhibited very high gas permeability. Particle dispersion was characterized using transmission electron microscopy (TEM). Nanocomposite density and gas permeation properties of CO_2, CH_4, N_2, and H_2 are reported as a function of particle concentration. Nanocomposite physical aging was also studied by monitoring the changes in gas permeability over time. For all of the gases except H_2, gas solubility was also measured. From the measured permeability and solubility data, gas diffusion coefficients were calculated.

2. Background

2.1. Gas transport

The steady-state gas permeability of gas A, P_A, is the pressure and thickness normalized flux [19]:

$$P_A = \frac{N_A l}{p_2 - p_1} \tag{1}$$

where p_1 and p_2 are gas pressures at the downstream and upstream film surfaces, respectively, l is film thickness, and N_A is the steady-state flux of gas A across the film. If Fick's Law is obeyed, the flux can be written as follows [19]:

$$N_A = \frac{C_2 - C_1}{l}\overline{D} \tag{2}$$

where C_1 and C_2 are the gas concentrations in the polymer at the downstream and upstream film surfaces, respectively, and $\overline{D}$ is the concentration averaged effective diffusion coefficient. Substituting Eq. (2) into Eq. (1) yields [19]:

$$P = \left(\frac{C_2 - C_1}{p_2 - p_1}\right)\overline{D} \tag{3}$$

Often, C_2 and p_2 are much greater than the downstream concentration and pressure, so Eq. (3) can be written as [20]:

$$P = \frac{C_2}{p_2}\overline{D} \tag{4}$$

The ratio of sorbed gas concentration to pressure is the apparent solubility coefficient of the penetrant in the polymer matrix, S [19]:

$$S = \frac{C_2}{p_2} \tag{5}$$

The ideal selectivity is defined as [19]:

$$\alpha_{A/B} = \frac{P_A}{P_B} \tag{6}$$

2.2. Particle loading

Generally, nanocomposite properties are reported as a function of weight fraction or weight percent of nanoparticles included in the sample [2,5,21,22]. However, due to density differences between the particles and polymer, nanoparticle volume percent provides a more relevant measure of the region of the sample occupied by particles. However, data are relatively rarely reported as a function of particle volume fraction because the conversion of weight fraction, which is the quantity that can be measured experimentally, to volume fraction requires assumptions of the appropriate values of polymer and particle density. The appropriate density values can be difficult to ascertain, particularly if the particles alter the polymer chain packing, thereby changing the polymer density or introduce voids, which cannot be accounted for properly using weight fraction data alone. In a recent paper, we defined the nominal volume fraction of filler, ϕ_F^N, as follows [23]:

$$\phi_F^N = \frac{V_F}{V_P + V_F} \tag{7}$$

where V_P and V_F are the ideal contributions of the polymer and filler, respectively, to the total volume, defined as the mass of polymer (M_P) or filler (M_F) added to the composite, divided by the pure polymer or filler density (ρ_P and ρ_F, respectively), that is:

$$V_P = \frac{M_P}{\rho_P} \tag{8}$$

and

$$V_F = \frac{M_F}{\rho_F} \tag{9}$$

Due to the possible presence of void space (*i.e.*, additional free volume, areas of poor wetting or dewetting at the particle–polymer interface, *etc.*) the nominal free volume does not always accurately predict the true volume fraction filler,

ϕ_F^T. To calculate ϕ_F^T, we first compare the measured nanocomposite density, ρ_{Exp}, to that predicted by the following additive model, ρ_{Add} [23]:

$$\rho_{Add} = \rho_F \phi_F^N + \rho_P \left(1 - \phi_F^N\right) \tag{10}$$

Then the void volume fraction, ϕ_V, in the film is defined as [23]:

$$\phi_V = 1 - \frac{\rho_{Exp}}{\rho_{Add}} \tag{11}$$

The void volume fraction captures any deviations between the experimentally observed and additive densities of the nanocomposite. ϕ_V can be used to estimate the true volume fraction of nanoparticles in the nanocomposite, ϕ_F^T [23]:

$$\phi_F^T = \phi_F^N (1 - \phi_V) \tag{12}$$

In this study, the nominal volume percent filler is typically reported because it is closely related to the amount of polymer and particles used in preparing the samples. However, Eq. (12) can be used to calculate the true volume fraction of particles in the resulting composite.

2.3. Modeling gas transport properties in heterogeneous films

Bruggeman's model, which has been used to describe permeability in polymer composites over a wide range of dispersed phase concentrations, is given by [9–11]:

$$\frac{(P_C/P_M) - (P_D/P_M)}{1 - (P_D/P_M)} \left(\frac{P_C}{P_M}\right)^{-1/3} = 1 - \phi_D \tag{13}$$

where P_C, P_M, and P_D are the permeabilities of the composite, polymer matrix, and dispersed phase, respectively. ϕ_D is the dispersed phase volume fraction. When P_D is much less than P_M (*i.e.*, when the dispersed phase is impermeable), Bruggeman's model becomes [10]:

$$\frac{P_C}{P_M} = (1 - \phi_D)^{3/2} \tag{14}$$

when P_D is much greater than P_M, Eq. (13) reduces to [10]:

$$\frac{P_C}{P_M} = \frac{1}{(1 - \phi_D)^3} \tag{15}$$

3. Materials and methods

Spherical MgO (*i.e.*, periclase) nanoparticles (Nanoscale, Manhattan, KS) were used in this study. According to the manufacturer, MgO has a crystalline density of 3.58 g/cm^3. The BET surface area is reported by the manufacturer to be between 600 and 650 m^2/g, which corresponds to a particle diameter of about 3 nm. Poly(1-trimethylsilyl-1-propyne), kindly supplied by Air Products and Chemicals (Allentown, PA), had a density of 0.75 g/cm^3 [24]. CH_4, H_2, CO_2, N_2, and *n*-butane were obtained from Airgas (Radnor, PA). Each gas was at least 99% pure as reported by the manufacturer. The nanoparticles, PTMSP, and gases were used as-received.

Prior to preparing the sample solution, all glasswares were dried in an oven at 80 °C overnight and allowed to cool to room temperature under an N_2 atmosphere to reduce the introduction of adventitious water, which can react with MgO, from the glassware into the sample solutions [25]. PTMSP was dissolved in toluene. As-received from the supplier, toluene contained 50 ppm H_2O and included molecular sieves to minimize its water content (Acros Organics, Geel, Belgium). The polymer/solvent mixture was stirred until the polymer dissolved, which generally took two days. The solution was transferred to a glove box under an N_2 atmosphere to reduce subsequent nanoparticle exposure to atmospheric humidity. Nanoparticles were added to the solution to yield a final dry film having a predetermined nominal volume percent, ϕ_F^N, of particles based on Eq. (7). The particle-filled solution was then mixed, using a magnetic stir bar, for at least 18 h at ambient conditions. The solution was poured onto a clean, dry, level glass plate and dried under a dry N_2 blanket in a glove box swept with N_2 at room temperature and at a pressure of 2 inches of H_2O in excess of atmospheric pressure. Complete evaporation of toluene usually required less than two days. The resulting nanocomposite films were approximately 200 μm thick after casting. Gas permeability was independent of thickness in the range explored (100–300 μm).

Solution cast PTMSP and nanocomposite films were ultramicrotomed to prepare sample cross-sections for atomic force microscopy (AFM), as described elsewhere [23,26]. Samples were polished using a microtome to produce a small protruding rectangular surface. PTMSP based samples were polished at room temperature at 0.6 mm/s using a Leica Ultracut UCT from Leica Microsystems GmbH (Wetzlar, Hesse, Germany) equipped with a diamond knife from Micro Star Technologies (Huntsville, TX). The samples were mounted with the polished side facing the AFM probe and perpendicular to the probe movement.

A Digital Instruments Dimension 3100 AFM with Nanoscope IV controller (Woodbury, NY) using silicon NCH AFM tips from Nanoworld (Neuchatel, Switzerland) in tapping mode was used to obtain phase profiles of particle distributions in the nanocomposite cross-sections. Phase profiles were obtained over a 1 μm by 1 μm surface area with 512 lines scanned per sample, which yielded a resolution of 2 nm per line. The scan rate was 0.8 Hz. The integral feedback was set to 0.2 and the proportional feedback was set to 1.0.

Nanocomposite samples were prepared for transmission electron microscopy (TEM) by embedding trimmed nanocomposite cross-sections in LR White resin (Electron Microscopy Sciences, Hatfield, PA) by cold curing in a BEEM® capsule container (Ted Pella Inc., Redding, CA). Embedded samples were pre-trimmed using a glass knife at room temperature with a Leica Ultracut UCT microtome (Leica Microsystems GmbH, Wetzlar, Hesse, Germany) to form a small, protruding, truncated pyramidal shape containing the sample, with

a smooth rectangular face approximately 100–200 μm in length and width. 50 nm thick sections were cut from the pyramid using a diamond knife (Micro Star Technologies, Huntsville, TX) at a rate of 0.6 mm/s. The cut sections floated on water in a diamond knife boat and they were collected with 400-mesh copper TEM grids (Ted Pella Inc.). Transmission electron microscopy, using a FEI TECNAI G^2 F20 TEM (FEI Company, Hillsboro, OR), was performed at an accelerating voltage of 200 kV at room temperature.

Density was measured via a hydrostatic weighing method using a Mettler Toledo balance (Model AG204, Columbus, OH) and a density determination kit [27]. Samples were tested in deionized water (18.2 MΩ) prepared using a Milli-Q plus TOC water purification system (Millipore, Billerica, MA).

Pure gas permeability coefficients were determined using a constant pressure/variable volume apparatus [28]. Permeation experiments were conducted on pure polymer and nanocomposite films that were approximately 200 μm thick and had a surface area of 13.8 cm^2. The film was exposed to test gases and the data were collected once steady-state conditions were established. The gas permeability coefficient (cm^3(STP) cm/(cm^2 s cm Hg)) was calculated from the steady-state permeate flow rate through a bubble flow meter according to the following equation [29]:

$$P_A = \frac{273 p_{atm}}{76T} \frac{l}{A(p_2 - p_1)} \frac{dV}{dt} \tag{16}$$

where l is the film thickness (cm), dV/dt is the permeate volumetric flow rate (cm^3/s), p_2 is the feed absolute pressure, p_1 is the permeate absolute pressure, p_{atm} is the atmospheric absolute pressure (cm Hg), T is the absolute temperature (K), and A is the film area available for transport (cm^2). The coefficient 273/76 corrects the measured permeate gas flow rate to cm^3 (STP). All experiments were performed at atmospheric downstream pressure. Permeability is often reported in units of barrer, which is defined as:

$$1 \text{ barrer} = 10^{-10} \frac{cm^3(STP)cm}{cm^2 \text{ s cm Hg}} \tag{17}$$

The permeability values reported in this manuscript are often reported in units of kilobarrer (kbarrer), which is 1000 barrer.

Kinetic gravimetric sorption experiments were used to characterize the adsorption of CO_2, CH_4, and N_2 onto nanoparticles. For these studies, an automated spring balance system, as described elsewhere, was used [30]. A Mettler Toledo balance was used to determine the nanoparticle weight at ambient conditions in air. The nanoparticle sample was loaded in a hemispherical quartz pan, which was suspended on a quartz spring from Ruska Instruments (Houston, TX) having a known spring constant. An initial spring extension reading was recorded at atmospheric pressure in air. Vacuum was applied for at least 18 h to degas the particles and the sorption chamber. A second spring extension reading was made to determine the weight loss due to desorption of gases from the nanoparticle sample.

To begin an adsorption experiment, a charge chamber was filled with approximately 4 cm Hg of gas. Once the charge gas reached the experimental temperature (*i.e.*, 35 °C), the sample chamber was slowly filled with gas from the charge chamber. Gas adsorption generally reached equilibrium within 20 min. Once the equilibrium spring extension had been recorded, an additional 10 cm Hg of gas at 35 °C was admitted to the sample chamber from the charge chamber. This process was repeated until the system pressure was just below atmospheric pressure (the test limit for this apparatus). Gas concentration on the particles, C_f (cm^3(STP)/cm^3 particles), was calculated as follows:

$$C_f = \frac{22{,}414 \rho_F k (l_p - l_v)}{W_F M_w} \tag{18}$$

where W_F is the filler mass (g), ρ_F is the nanoparticle density (g/cm^3), and l_p and l_v are the spring extension at equilibrium at a given pressure and at equilibrium in vacuum (mm), respectively. M_w is the test gas molar mass (g/mol). k is the spring constant, which was 2.82×10^{-4} g/mm in these experiments. The constant 22,414 has units of cm^3(STP)/mol of gas.

A high-pressure barometric sorption apparatus [31,32] was used to determine gas sorption in unfilled (*i.e.*, neat) PTMSP and MgO filled nanocomposites. Prior to beginning these experiments, vacuum was applied to the sorption apparatus containing the sample for at least 18 h to degas the sample. The degassed sample was then exposed to pure N_2, CH_4, and CO_2, in that order, at intervals of approximately 3 atm from vacuum to 20–30 atm at 35 °C, and gas solubility values were determined from the resulting experimental data as described in the literature [31,32].

4. Results and discussion

4.1. Polymer–particle interactions

In the presence of water, periclase nanoparticles and PTMSP undergo a chemical reaction that results in partial desilylation of the polymer [25]. The desilylation reaction removes, at most, approximately 9 percent of the trimethylsilyl groups from PTMSP [25]. The sample preparation protocol discussed above was developed to minimize the reaction between the polymer and particles by limiting sample exposure to adventitious water. In the samples considered in this study, WAXD studies confirm that the particle structure did not change from periclase to brucite, which would be observed if the particles had reacted with water [25]. The hydration reaction of MgO (*i.e.*, the conversion of periclase to brucite) is the first step in the reaction of the particles with the polymer [25]. Additionally, FTIR and ^{1}H NMR studies did not show any evidence of reaction between the particles and polymer. Based on this experimental protocol, any reaction between the polymer and particles was at a level that was below the detection limit of FTIR and ^{1}H NMR, which were used previously to characterize the reaction of these particles with PTMSP [25].

4.2. Characterization of particle dispersion

Nanoparticle dispersion strongly influences gas transport properties in heterogeneous films. For instance, incorporation of trimethylsilylglucose reduces gas permeability in PTMSP by up to 99% relative to that of unfilled PTMSP [33]. In contrast, permeability increases substantially when brookite nanoparticles are added to PTMSP [23]. The influence of particles on transport properties is determined, in part, by the degree of dispersion of the particles in the polymer. When the particles disperse individually or in nanometer-scale aggregates, tapping mode phase profile AFM has been used to observe nanoparticle dispersion in PTMSP at a resolution of around 2 nm [23]. In PTMSP filled with TiO_2 and 1,2-polybutadiene filled with MgO nanoparticles, AFM revealed that at least some of the nanoparticles were dispersed individually [23,34]. However, for MgO dispersed in PTMSP, this was not the case. There were no individual nanoparticles or nanometer-scale aggregates of particles observed in these samples, suggesting that the MgO particles did not disperse as completely in PTMSP as other particles in PTMSP or as MgO in other polymers [23,34].

Fig. 1 presents TEM images of PTMSP filled with MgO nanoparticles. Even at low nanoparticle loading (*i.e.*, 5 nominal volume percent), the nanoparticles (*i.e.*, the dark regions in Fig. 1) form micron-sized aggregates, suggesting that these particles are dispersed into aggregates that are many times the size of individual particles. This result is in contrast to other nanocomposites, such as PTMSP filled with TiO_2 or 1,2-polybutadiene filled with MgO, which exhibit a substantial amount of nanometer-sized particle aggregates at similar loadings [23,34]. The TEM images also show numerous micron-sized voids (*i.e.*, light gray areas in the TEM images). It is not clear if these voids are artifacts caused by the microtoming during the sample preparation or if they are an inherent feature of the dispersion of MgO particles in PTMSP.

A number of factors probably contribute to the observed wide variation in the degree of dispersion of nanoparticles in different polymers and to the possibility of void formation, such as particle–polymer interactions, casting conditions, polymer chain stiffness, particle loading, *etc*. Currently, there is not enough information available to definitively predict which particles will disperse well in which polymers and whether or not small scale voids (to be discussed in the next section) will be formed in the resulting nanocomposite samples.

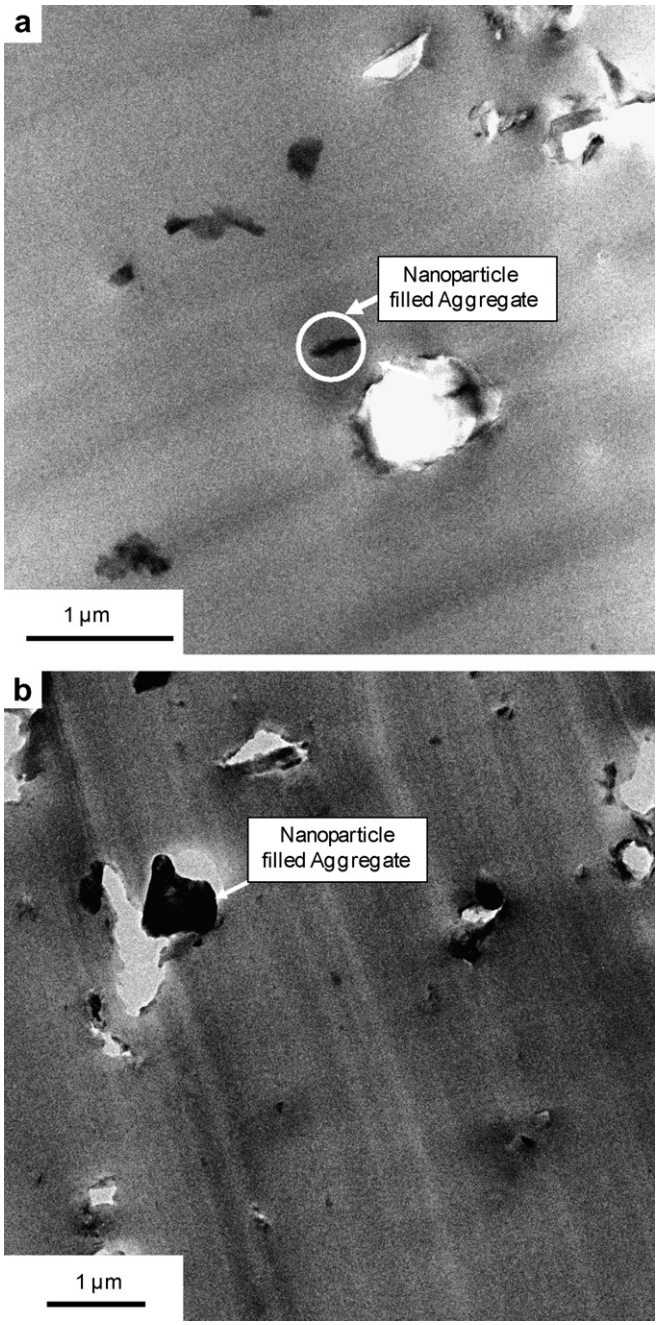

Fig. 1. TEM images of PTMSP containing (a) 5 and (b) 10 nominal volume percent MgO.

4.3. Density and voids in nanocomposite samples

Fig. 2 presents the density of nanocomposite samples as a function of particle loading. A notable feature of Fig. 2 is that free-standing nanocomposite films may be prepared at loadings as high as 75 nominal volume percent particles, which correspond to 94 wt. % particles in the polymer. To the best of our knowledge, such high loadings of particles in polymers considered for gas permeation properties have not been reported previously. Often, as inorganic particle content increases, polymer-based composites become brittle and, therefore, too fragile to test in gas permeation experiments, or the samples develop transmembrane defects that render the materials non-selective in gas permeation tests [23,35,36]. So, most studies do not report samples with particle loadings as high as those discussed in this study. For example, the maximum zeolite 4A content in poly(vinyl acetate) considered by Mahajan and Koros was 40 wt.% before samples could no longer be prepared without selectivity-destroying defects [35]. While there is no evidence of chemical reaction between the particles and the polymer, the ability to reach such high loadings suggests somewhat favorable interactions between the particles and the polymer.

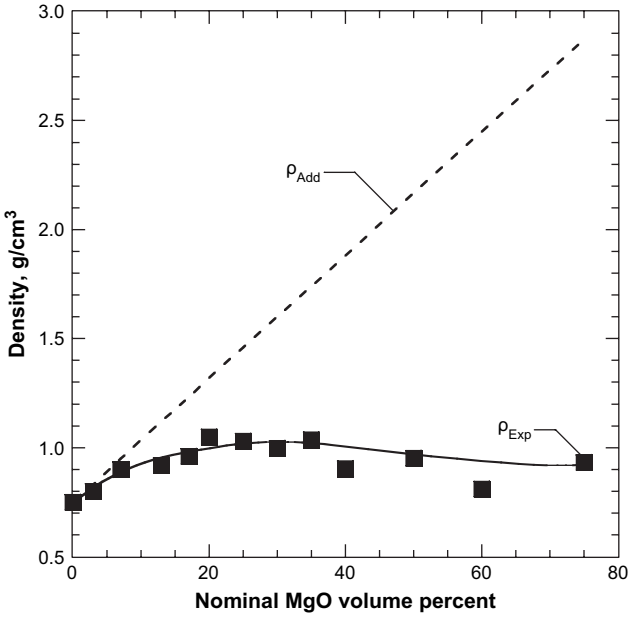

Fig. 2. Effect of MgO concentration in nanocomposites on density (ρ_{Exp}, ■). The dashed line represents the additive density, ρ_{Add}, as calculated by Eq. (10). The solid trend line is drawn to guide the eye.

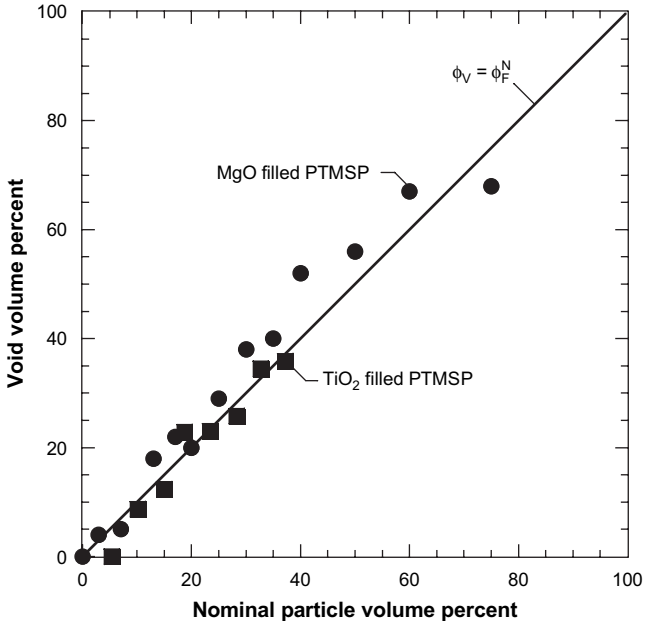

Fig. 3. Correlation between particle loading and void volume percent in PTMSP/MgO (●) and PTMSP/TiO_2 (■) nanocomposite films [23]. The solid line represents $\phi_V = \phi_F^N$.

The simplest model of nanocomposite density would be that in which the nanocomposite density, ρ_{Add}, would obey an additive model, such as Eq. (10) [23]. However, as indicated by the density data in Fig. 2, the PTMSP/MgO system shows significant deviations from this model. The experimentally observed density is considerably lower than that expected based on the additive model, and the deviation between the data and the model increases as particle concentration increases. These data strongly suggest that these nanocomposite samples contain rather high levels of voids, either within the polymer or particle phases or at the interface between them.

The deviation between the additive model and the experimental density can be quantified in terms of the volume fraction of voids, ϕ_V, as calculated using Eq. (11) [23]. Fig. 3 presents the effect of nanoparticle concentration on void volume percent in PTMSP containing MgO and in PTMSP/TiO_2 nanocomposites based on TiO_2 nanoparticles having a primary particle diameter of approximately 3 nm [23]. Interestingly, the trend in void volume with particle loading does not depend on particle type. The void volume percent increases with increasing particle loading to the point where the composite materials are mainly void space at high particle loadings. The line shown in this figure corresponds to the case where the void volume and nominal particle volume percent are equal. While it is not clear why the void volume and nominal particle volume percent are equal, it is interesting that this trend is observed. The location of the voids within the nanocomposite could not be identified using common microscopic techniques, but the existence of void space in mixed matrix polymer-based materials has been reported in the literature for a variety of particle–polymer combinations [3,9,13,22]. The data in Fig. 3 extend significantly farther for MgO-based composites than for TiO_2-based composites because the TiO_2 samples exhibit non-selective permeation (*i.e.*, defects) in the films when the nominal volume fraction is above 38%, providing another indication that the interactions between the polymer and particles more strongly favor preparation of samples with high particle loadings in the MgO case.

The true volume fraction of particles in the nanocomposite, ϕ_F^T, which is the volume of particles per unit volume of sample (including polymer, particles, and void space) can be calculated using Eq. (12). For the samples considered in this study, the maximum value of the true volume percent of particles was 24 percent at 75 nominal volume percent MgO, which is well below the maximum packing limit for spherical particles in a matrix, which is 49 volume percent [37].

4.4. Gas permeability in PTMSP/MgO nanocomposites

Generally, dispersing impermeable particles in polymer matrixes decreases gas permeability [9,15,33]. However, this trend is not always obeyed in nanoparticle-filled polymers. Nanoparticles can disrupt chain packing in glassy polymers, thereby increasing free volume in the polymer phase, which acts to increase permeability [2]. In other heterogeneous systems, voids at the polymer–particle interface or between particles in particle aggregates cause permeability to be greater in nanocomposites than in unfilled polymers [22,23]. In this regard, Fig. 4 shows strong increases in gas permeability in PTMSP as MgO loading increases. The unfilled PTMSP permeability values at $\Delta p = 3.4$ atm are 35, 18, 7, and 18 kbarrer for CO_2, CH_4, N_2, and H_2, respectively. These values are similar to those reported in the literature. For instance, Pinnau and Toy report CO_2, CH_4, N_2, and H_2 permeability values at 23 °C and $\Delta p = 3.4$ atm of 34, 16, 6, and 17 kbarrer, respectively

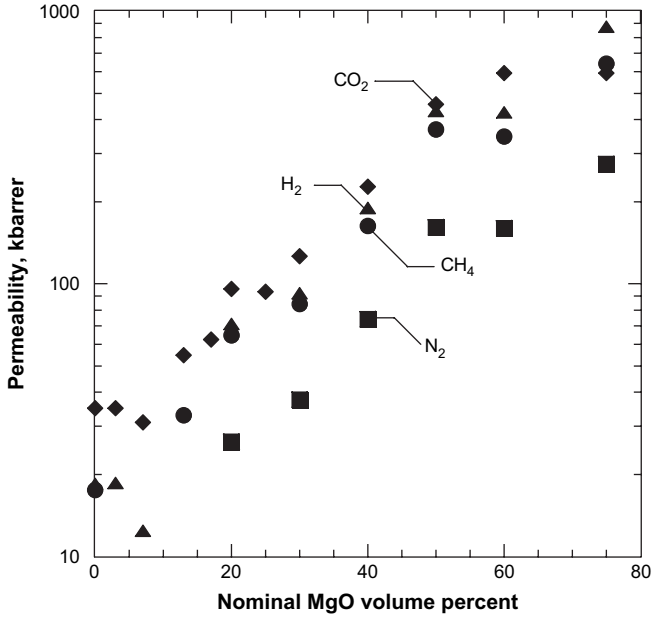

Fig. 4. Effect of MgO concentration on CO_2 (◆), CH_4 (●), N_2 (■), and H_2 (▲) permeability at $\Delta p = 3.4$ atm. These measurements were made at 35 °C and atmospheric downstream pressure.

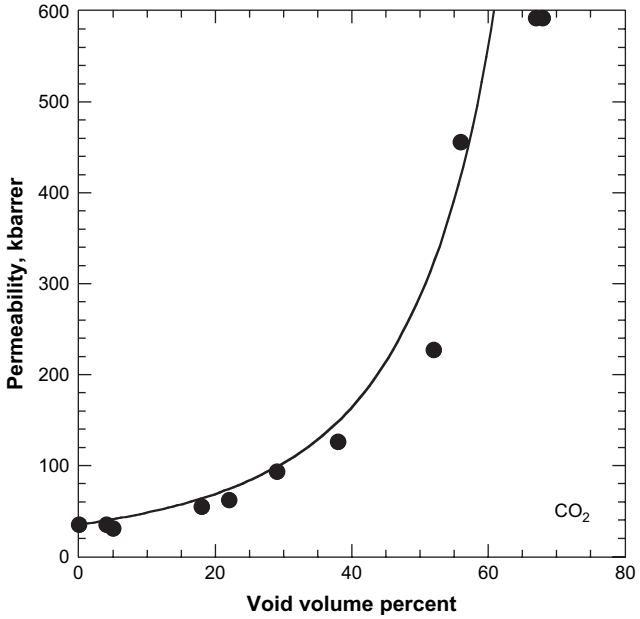

Fig. 5. Effect of void volume, ϕ_V, on CO_2 permeability (●) at $\Delta p = 3.4$ atm. The solid line represents Eq. (15), where the voids are treated as the dispersed phase (*i.e.*, setting $\phi_D = \phi_V$ in Eq. (15)). These measurements were made at 35 °C and atmospheric downstream pressure.

[38]. At the highest particle loadings in Fig. 4, which correspond to 94 wt.% particles, the CO_2, CH_4, N_2, and H_2 permeability coefficients are 17, 28, 30, and 40 times higher than that in unfilled PTMSP.

Fig. 5 presents a correlation of the CO_2 permeability with void volume. Applying Bruggeman's model in the limit where the dispersed phase (the voids, in this case) is much more permeable than the matrix phase (*i.e.*, setting $\phi_V = \phi_D$ in Eq. (15)), one obtains a reasonable fit of the experimental permeability data to the model, as indicated in Fig. 5. There are no adjustable parameters in Eq. (15). Similar comparisons for the other gases are provided in Supplementary information (Supplementary Fig. 1), and they are consistent with the results in Fig. 5. The dependence of gas permeability on the amount of void space in the nanocomposites is similar among a variety of nanoparticle fillers dispersed in PTMSP. For instance, CO_2 permeability values in PTMSP filled with either MgO or TiO_2 nanoparticles are similar at the same void volume content, as demonstrated in Fig. 6 [23]. Similar results have been observed for the other gases considered in this study and the results are presented in Supplementary information (Supplementary Fig. 2). Therefore, the basic permeation properties of the polymer are not affected by the presence of the particles or, at least, any change in polymer transport properties is overshadowed by the dominant effect of the voids on the permeability of the nanocomposites.

The permeability coefficients in PTMSP/MgO nanocomposites are very high. For instance, in PTMSP containing 75 nominal volume percent MgO, CO_2 permeability is ~600 kbarrer at $\Delta p = 3.4$ atm and 35 °C, and *n*-butane permeability is 1200 kbarrer at $\Delta p = 0.9$ atm and 35 °C. A key question is whether the observed permeability coefficients are consistent with gas transport in a polymer without transmembrane defects or whether the results are simply due to the particle's ability, particularly at high loadings, to introduce defects that span the sample.

Permeability in systems exhibiting Poiseuille flow, which would be observed if large defects (*i.e.*, >50 nm or so [39]) were present in the films, would typically increase with increasing pressure difference across the film [40]. Fig. 7

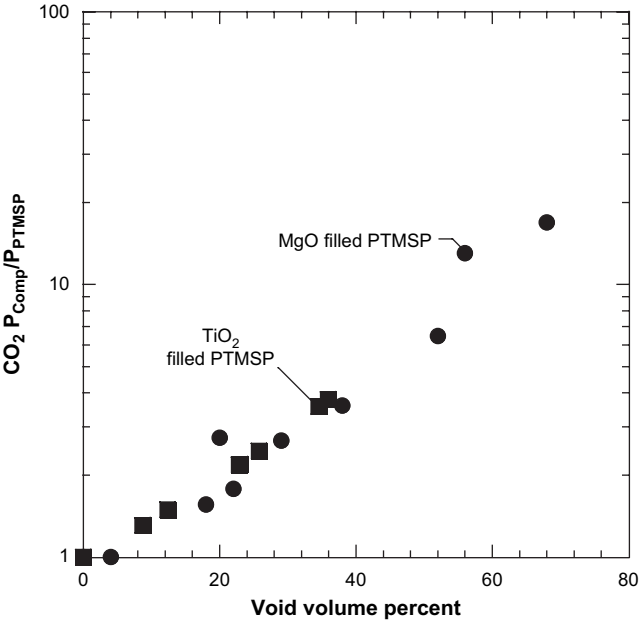

Fig. 6. Effect of void volume percent, as calculated by Eq. (11), on the ratio of CO_2 permeability in the nanocomposite, P_{Comp}, to CO_2 permeability in PTMSP, P_{PTMSP}, in PTMSP/MgO (●) and PTMSP/TiO_2 (■) nanocomposite films [23].

presents permeability coefficients in PTMSP nanocomposites containing MgO. CO_2 and CH_4 permeability in unfilled PTMSP decreases slightly with increasing pressure, which is consistent with the reports in the literature [23,29]. However, the decrease in permeability with increasing CO_2 and CH_4 pressure is small enough to be masked by the scale of Fig. 7a and 7b. In summary, gas permeability does not increase with increasing upstream pressure, which indicates that the gas transport behavior does not obey Poiseuille flow.

Gas selectivity values provide further evidence regarding the presence of selectivity-destroying defects in the PTMSP/MgO nanocomposites. Depending upon the defect or pore size, in a polymer film containing a pore or defect that is connected across the entire sample, the ideal selectivity can reach the Poiseuille limit, $\alpha^{P}_{A/B}$, if the pores are large enough or the Knudsen limit, $\alpha^{K}_{A/B}$, if the pores are smaller [39]. $\alpha^{P}_{A/B}$ is [40,43]:

$$\alpha^{P}_{A/B} = \frac{\mu_B}{\mu_A} \tag{19}$$

where μ_A and μ_B are the viscosities of gases A and B, respectively. The selectivity values presented in this study were calculated as the ratio of pure gas permeability coefficients (*cf.*, Eq. (6)). Therefore, the selectivity in Eq. (19) is based on the ratio of pure gas permeability coefficients for a pair of gases undergoing Poiseuille flow in a cylindrical tube [40,43]. Obviously, if mixtures of gases were copermeated in Poiseuille flow through a cylindrical tube, the selectivity would be 1 (*i.e.*, the flow would be non-selective) [40]. The Knudsen selectivity limit, $\alpha^{K}_{A/B}$, is [43]:

$$\alpha^{K}_{A/B} = \sqrt{\frac{M_B}{M_A}} \tag{20}$$

where M_A and M_B are the molecular masses of gases A and B, respectively. Poiseuille and Knudsen flow selectivity limits are presented in Table 1 for the gas pairs of interest to this study. The viscosity data used to generate the selectivity values in Table 1 are at 35 °C [44].

The selectivity data provide some information regarding the transport mechanism governing gas transport in these

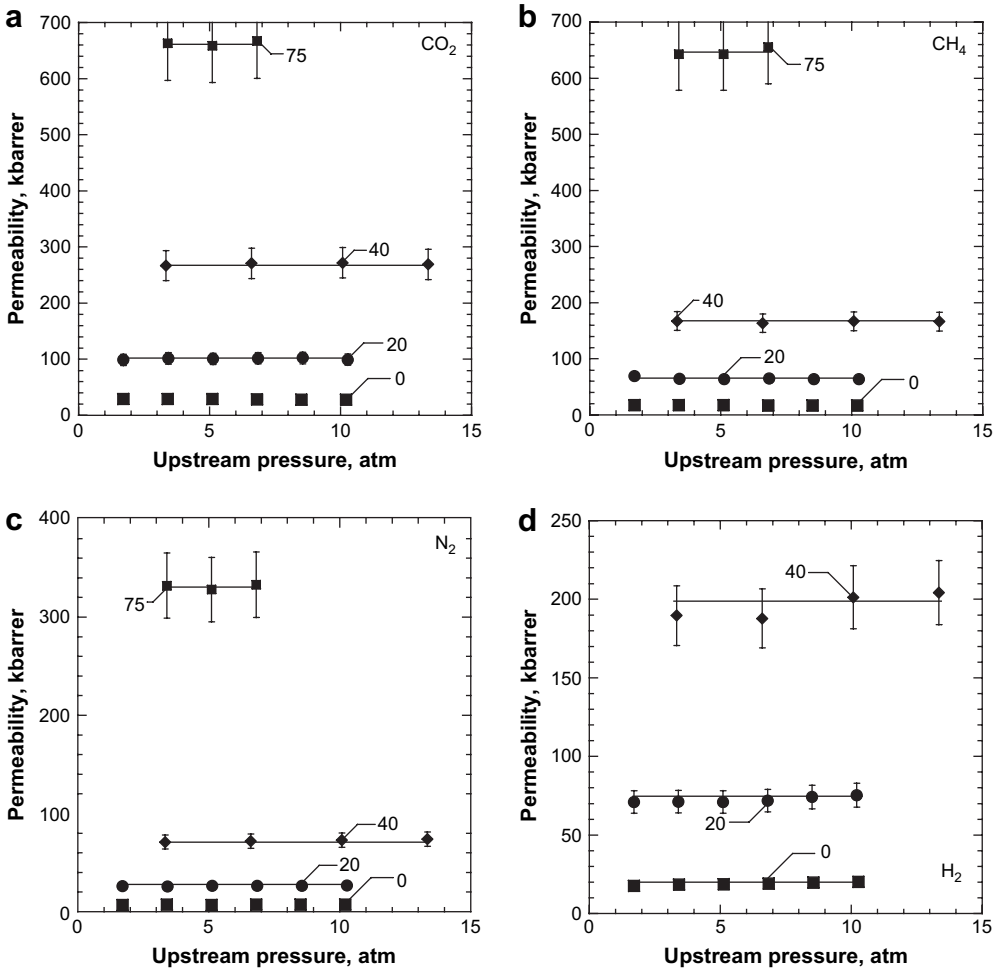

Fig. 7. Effect of upstream pressure on pure gas permeability of PTMSP containing various nominal volume percents, ϕ^{N}_{F}, of MgO for (a) CO_2, (b) CH_4, (c) N_2, and (d) H_2. These measurements were conducted at 35 °C and at atmospheric downstream pressure. Error bars were estimated from the variance in permeability for multiple experiments at each loading and pressure according to the propagation of errors method described by Bevington and Robinson [41]. The solid lines are drawn to guide the eye.

Table 1
Knudsen diffusion and Poiseuille flow selectivities

Flow regime	CO_2/N_2	CO_2/CH_4	CO_2/H_2	H_2/N_2	H_2/CH_4	CH_4/N_2
Knudsen diffusion	0.8	0.6	0.2	3.7	2.8	1.3
Poiseuille flow	1.2	0.7	0.6	2.0	1.2	1.7

nanocomposite samples and changes in transport mechanism with particle content. In this regard, Fig. 8 presents the pure gas selectivity values as a function of particle content. Interestingly, the CO_2/CH_4, CO_2/N_2, and CO_2/H_2 selectivity values generally decrease with increasing particle content. In contrast, the H_2/N_2 and H_2/CH_4 selectivity values increase somewhat with increasing particle content. The CH_4/N_2 selectivity exhibits little to no change with particle content. In each of these cases, as the particle content increases, the selectivity values trend towards, but do not reach, selectivity values expected based on Knudsen flow (*cf.*, Table 1). These results suggest that as particle content increases, transport in the nanocomposites becomes more similar to transport through interconnected pores, of a size characteristic of that required for Knudsen flow [39,43], that span the sample. For some of the gas pairs (*e.g.*, H_2/CH_4 and CO_2/H_2) the selectivity values also achieve values consistent with Poiseuille flow. For the other gas pairs, this is not the case. Given that the permeability coefficients do not exhibit the pressure dependence expected for Poiseuille flow, it is unlikely that this flow mechanism is active in these materials.

These results appear to be consistent with those reported earlier by Merkel et al. For example, they observed that H_2/CH_4 increased from about 0.9 in PTMSP to 1.2 in PTMSP containing 50 wt.% fumed silica nanoparticles [39]. Merkel et al. argued that as nanoparticle content increased, contributions from pore flow modes of transport (*e.g.*, Knudsen flow) to the overall rate of gas transport became more important relative to solution-diffusion transport. Merkel et al. reasoned that in the transition from solution-diffusion to pore flow, the solubility selectivity, which in the solution-diffusion limit favors CH_4 in the case of H_2/CH_4, would tend to be unity, which is the value of the solubility selectivity expected for pore flow. This change in solubility selectivity would act to increase H_2/CH_4 permeability selectivity, which is consistent with the results shown in Fig. 8b. In this picture, the permeability selectivity would approach that of Knudsen transport as the contribution of pore flow to the overall gas transport increased (*i.e.*, as particle content increased). In the PTMSP/MgO case presented in Fig. 8b, the Knudsen selectivity limit (2.8 for H_2/CH_4) is not reached, suggesting that solution-diffusion transport still contributes substantially to the total rate of transport even in the nanocomposites containing the highest concentrations of particles. Similar reasoning would also explain why H_2/N_2 selectivity appears to exhibit a slight increase towards the Knudsen limit of 3.7 (*cf.*, Table 1) with increasing particle content. In the case of CH_4/N_2, the solubility selectivity in the polymer favors CH_4 [29], so transition to a pore flow regime would favor a reduction in permeability selectivity. However, this trend might be partially offset by the fact that in the solution-diffusion limit, nitrogen would typically be expected to have a higher diffusion coefficient than methane, since the kinetic diameter of nitrogen (3.64 Å) is slightly less than that of methane (3.8 Å) [45], while the situation would be reversed, with methane having the higher diffusion coefficient, in the Knudsen flow limit. The resulting combination of factors apparently acts to keep the selectivity largely unchanged as particle content increases.

In the case of the selectivity values involving CO_2 (*i.e.*, Fig. 8a), the solubility selectivity in the solution-diffusion limit always favors CO_2. Therefore, at higher particle contents, if there is a transition to pore flow modes of transport, such as Knudsen flow, the solubility selectivity favoring CO_2 would be lost, resulting in an overall decrease in selectivity, which is consistent with that observed in Fig. 8a. In each case, the selectivity decreases towards, but does not reach,

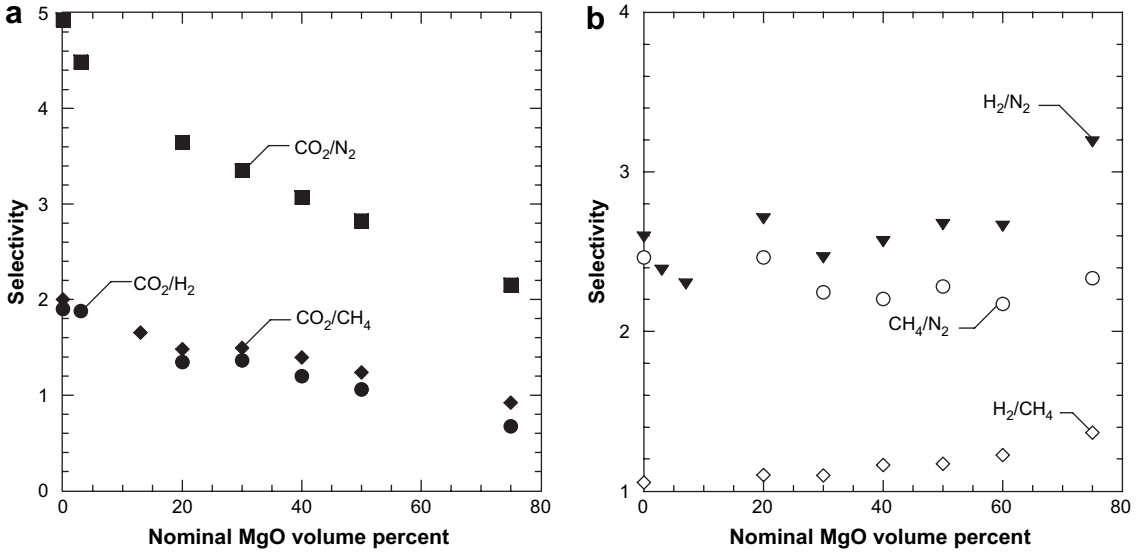

Fig. 8. Effect of MgO concentration on pure gas selectivities at $\Delta p = 3.4$ atm for (a) CO_2/N_2 (■), CO_2/CH_4 (◆), and CO_2/H_2 (●), as well as (b) H_2/N_2 (▼), H_2/CH_4 (◇), and CH_4/N_2 (○). Measurements were made at 35 °C and atmospheric downstream pressure.

Table 2
Freundlich isotherm parameters for adsorption onto MgO and dual mode sorption parameters for PTMSP at 35 °C

Penetrant	K, $\frac{cm^3(STP)}{cm^3\ MgO\ atm^{1/n}}$	n, –	k_D, $\frac{cm^3(STP)}{cm^3\ PTMSP\ atm}$	C'_H, $\frac{cm^3(STP)}{cm^3\ PTMSP}$	b, $\frac{1}{atm}$
N_2	31 ± 7	2.6 ± 0.2	0.1	74	0.014
CH_4	50 ± 8	2.5 ± 0.2	0.5	62	0.05
CO_2	63 ± 10	3.4 ± 0.2	1.1	130	0.04

Note: PTMSP dual mode parameters are from the literature [29]. Uncertainties in the Freundlich isotherm parameters were estimated as described in the literature [41].

selectivity values indicative of pore flow (*i.e.*, Knudsen diffusion). In summary, the permeability results are independent of pressure, suggesting that there are no large defects, which would allow flow mechanisms such as Poiseuille flow. However, the permeability selectivity results suggest a stronger influence of Knudsen flow on the overall transport properties as particle concentration increases.

In the remainder of this manuscript, the influence of particle concentration on gas permeability is analyzed further in terms of the influence of particle concentration on gas solubility and diffusivity using the solution-diffusion model, which presumes that the samples are free from trans-film defects. As a first step in this process, Fig. 9 presents gas sorption isotherms for the MgO nanoparticles alone. The Freundlich isotherm can adequately describe the adsorption of gases onto the particles, and this model is given by [34,46]:

$$C_f = Kp^{1/n} \tag{21}$$

where K and n are fitting parameters, and p is the gas pressure. Gas sorption in glassy polymers, C_p, typically obeys the dual mode sorption model [47,48]:

$$C_p = k_D p + \frac{C'_H bp}{1+bp} \tag{22}$$

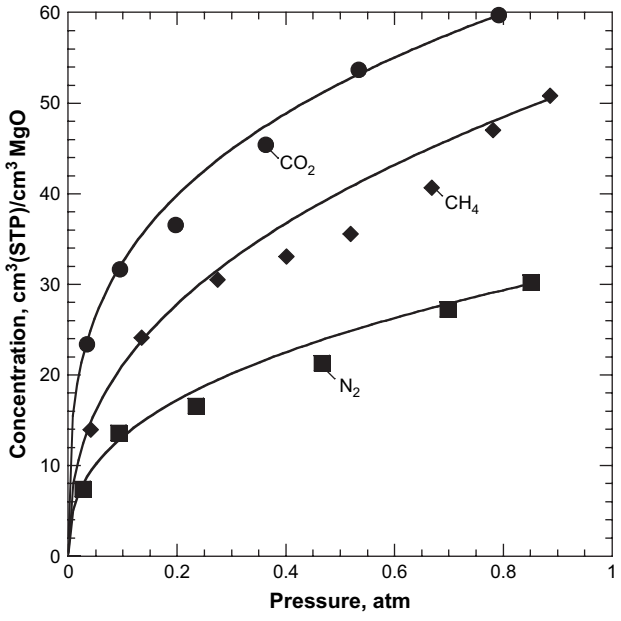

Fig. 9. Pure gas CO_2 (●), CH_4 (◆), and N_2 (■) adsorption isotherms on MgO at 35 °C. The lines represent the Freundlich model (*i.e.*, Eq. (21)).

where k_D is Henry's law constant, C'_H is the Langmuir sorption parameter, and b is the Langmuir affinity constant. Table 2 presents Freundlich isotherm parameters for CO_2, CH_4, and N_2 adsorptions on MgO nanoparticles from this study as well as dual mode parameters for PTMSP from the literature [29].

Fig. 10 presents sorption isotherms in unfilled PTMSP and nanocomposite samples. The sorption in unfilled PTMSP is in good agreement with that predicted by Eq. (22) using dual mode sorption parameters from the literature (*cf.*, Table 2) [29]. Due to the good agreement between sorption isotherms in the unfilled polymer with the literature data, the dual mode sorption model parameters from the literature are used in the calculation described below. In some, but not all, cases, the gas solubility in the nanocomposites is higher than in the unfilled polymer. Because the gas sorption levels are not a monotonic function of particle content, these results suggest that competing factors may contribute to the observed gas uptake. In the following paragraphs, these factors are discussed in more detail.

If the polymer and particles contributed their pure component gas sorption properties to the gas uptake in nanocomposite samples, then the gas sorption properties of the nanocomposite would obey the following additive model [9,23]:

$$C_C = \left(\phi_F^N C_f + \left(1-\phi_F^N\right)C_p\right)(1-\phi_V)C_V\phi_V \tag{23}$$

where C_C is the gas concentration in the nanocomposite ($cm^3(STP)/cm^3$ nanocomposite) and C_V is the concentration of gas in the voids, which is given by the ideal gas law [40]:

$$C_V = \frac{p}{RT} \tag{24}$$

To put this contribution in perspective with that of the polymer and particles (*cf.*, Table 2), the concentration of gas in a void at 35 °C and 1 atm would be 0.88 $cm^3(STP)/cm^3$ void, which is less than that of the gas concentration in the polymer or on the particles. Substituting Eqs. (21), (22), and (24) into Eq. (23) yields [23]:

$$C_C = \left(\phi_F^N K p^{1/n} + \left(1-\phi_F^N\right)\left(k_D p + \frac{C'_H bp}{1+bp}\right)\right)(1-\phi_V) + \frac{\phi_V p}{RT} \tag{25}$$

According to Eq. (25) and the data from Table 2, sorption on the nanoparticle surface and sorption into the polymer phase dominate the overall sorption of gas into the nanocomposite. For instance, for CO_2 sorption in a PTMSP film containing 13 nominal volume percent MgO (and 12 volume percent

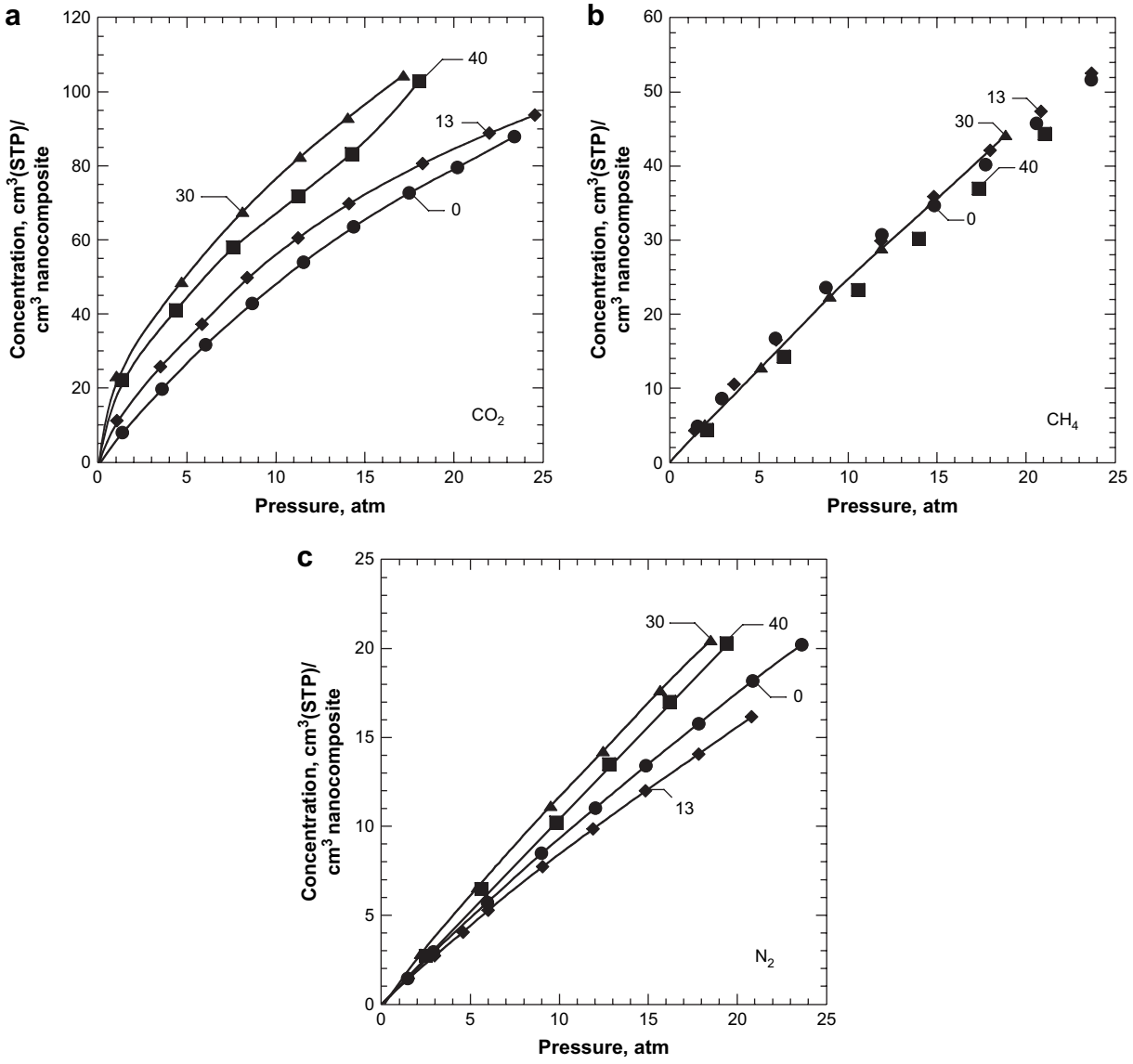

Fig. 10. Sorption isotherms at 35 °C for (a) CO_2, (b) CH_4, and (c) N_2 in PTMSP containing 0 (●), 13 (◆), 30 (▲), and 40 (■) nominal volume percent MgO nanoparticles. Trend lines are drawn to guide the eye in the nanocomposite samples. For pure PTMSP, the line through the data is the dual mode model (Eq. (22)) using the parameters shown in Table 2 [41].

voids) at 4.4 atm, adsorption on the nanoparticle surface (extrapolated from the experimental data in Fig. 9 and the Freundlich model) accounts for 47% of the overall sorbed gas concentration and sorption in the polymer phase accounts for 50% of the total sorbed gas concentration. In this case, the voids contribute only ~3% of the total sorbed gas in the nanocomposite. The contributions of particles, polymer, and voids to the total amount of gas uptake will vary with pressure, gas, and particle concentration. However, this example is a representative of the typical contributions of each phase to the gas concentration in the nanocomposites. Since the void volume makes a small, but non-negligible, contribution to the concentration of gas in the nanocomposite, certain nanocomposites adsorb less gas than the unfilled polymer (*cf.*, Fig. 10). In these cases, the increase in gas sorption due to incorporation of highly gas sorbing particles is more than offset by the low gas sorption in the voids. As indicated earlier, gas sorption levels in the voids, based on Eq. (24), are lower than gas sorption by either the polymer or particles.

At the same pressure, the gas concentration in nanocomposites containing 13 nominal volume percent particles is lower than the gas concentration in the unfilled polymer. This results from the manner in which gas concentration is normalized. The sorption isotherms in Fig. 10 are reported based on the concentration of gas in the nanocomposite volume (*i.e.*, in the entire volume of the sample, including polymer, particles, and void volume). When calculated in this fashion, the sorption isotherms do not follow a systematic trend with nanoparticle loading. However, sorption levels per unit volume of nanocomposite solids (*i.e.*, the polymer and particle volume, but not including the void volume) increase systematically with increasing particle loading, as shown in Fig. 11. These results appear reasonable, since the neat particles sorb more gas than the unfilled polymer.

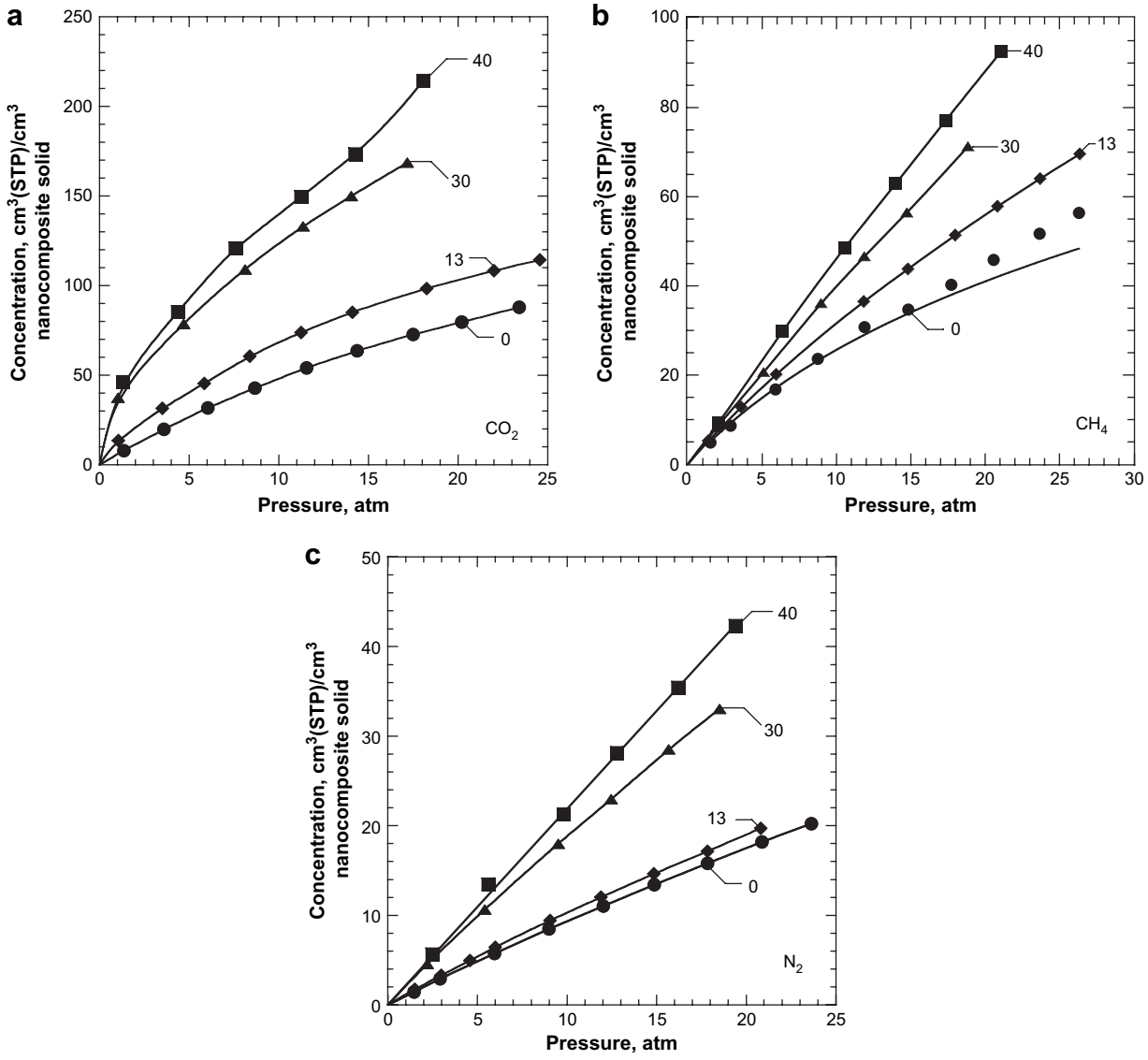

Fig. 11. Sorption isotherms in the nanocomposite solids for (a) CO_2, (b) CH_4, and (c) N_2 in PTMSP containing 0 (●), 13 (◆), 30 (▲), and 40 (■) nominal volume percent MgO nanoparticles at 35 °C. Trend lines are drawn to guide the eye in the nanocomposite samples. For pure PTMSP, the line through the data is the dual mode model (Eq. (22)) using the parameters shown in Table 2 [41].

Fig. 12 presents a comparison of Eq. (25) to experimental sorption data in a PTMSP/MgO nanocomposite containing 30 nominal volume percent MgO. Results for other particle concentrations are qualitatively consistent with those presented in Fig. 12 and additional examples are presented in Supplementary information (Supplementary Fig. 3). Eq. (25) overestimates the concentration of CH_4 and N_2, but it underestimates the CO_2 concentration in the nanocomposite. A reduction in gas sorption in polymer/inorganic particle composites relative to that predicted by an additive model such as Eq. (25) is often observed and has been ascribed to wetting of the particles by the polymer chains [9,23,49]. That is, any polymer chains that wet the particle surface occupy sorption sites that would otherwise be available to the gases, thereby reducing gas solubility in the composite below levels expected based on pure polymer and pure particle sorption properties [9].

It is not clear why Eq. (25) underestimates CO_2 concentration in the nanocomposites while it substantially overestimates the concentration of non-polar gases. However, CO_2 is the most strongly sorbing penetrant considered in this study, and MgO is basic [50], so it might have specific interactions with acidic CO_2 that are not accessible to CH_4 and N_2. Also, the low pressure sorption experiments used in this study may not accurately characterize the CO_2 sorption capacity of the MgO surface in the nanocomposites. For instance, Stark et al. report after preheating MgO nanoparticles overnight at 500 °C under vacuum, the nanoparticles sorbed approximately 150 cm^3(STP) CO_2/(cm^3 of nanoparticles) at 20 Torr (0.03 atm) and 23 °C [51], which indicates that MgO nanoparticles can sorb significantly more CO_2, depending on preparation method, than 60 cm^3(STP) CO_2/(cm^3 of nanoparticles) we report at 0.8 atm and 35 °C. Stark's sorption values may represent an upper limit to the concentration of CO_2 that can be adsorbed to MgO nanoparticles. It

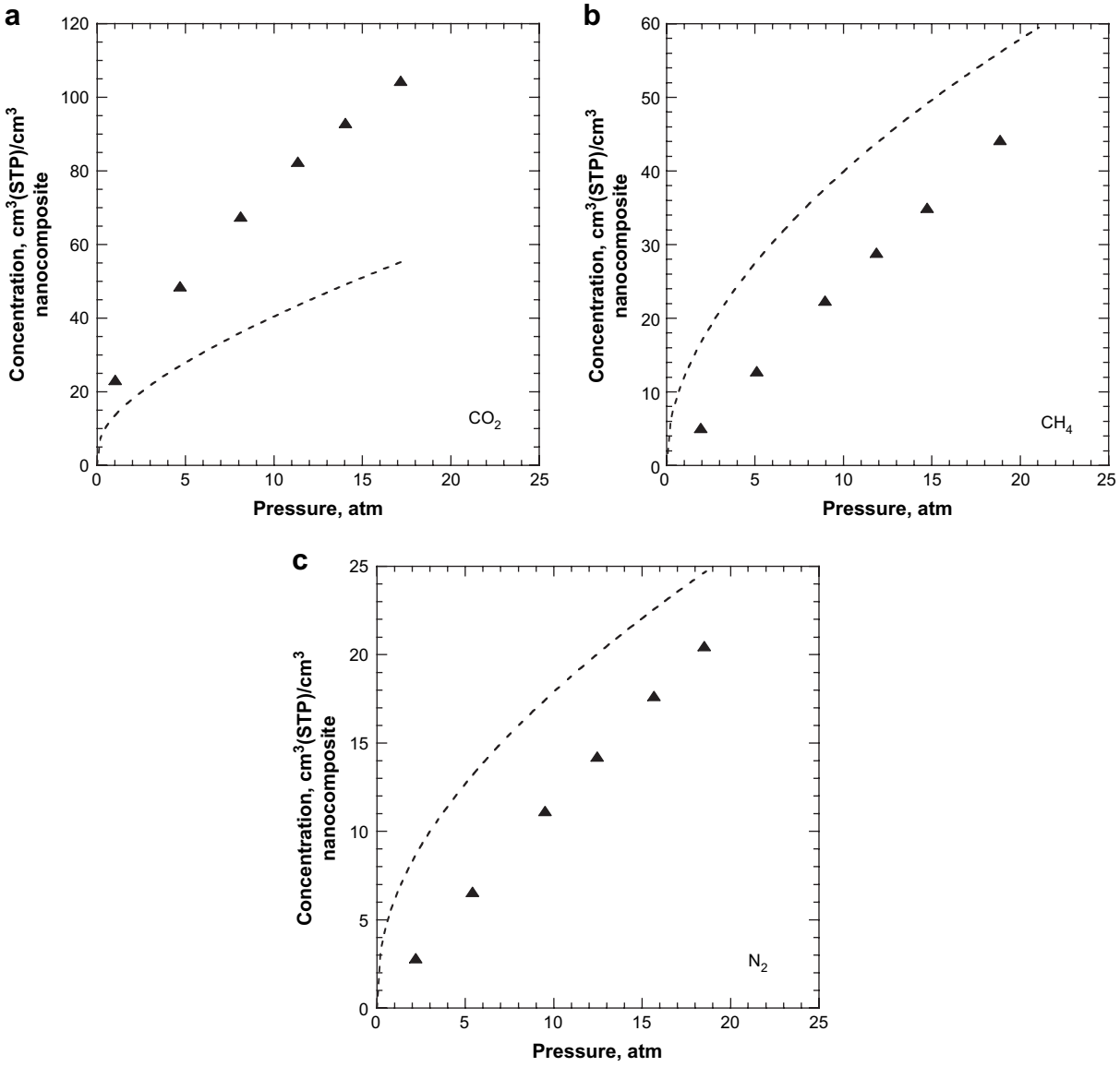

Fig. 12. Sorption isotherms of (a) CO_2, (b) CH_4, and (c) N_2 in a PTMSP nanocomposite containing 30 nominal volume percent MgO. The sorption level expected based on Eq. (25) using the parameters from Table 2 and void volume values from Fig. 3 is represented as dashed line.

is possible that the nanoparticles adsorb more CO_2 in the nanocomposites than the neat particles did during low pressure sorption experiments, which may account for the difference between the CO_2 sorption isotherms predicted by Eq. (25) and the CO_2 sorption isotherms determined experimentally. However, further studies, including high-pressure sorption studies of the gases onto the neat particles, which are not possible with our equipment, would be required to resolve this issue.

Since our adsorption studies of the particles could not be performed beyond atmospheric pressure, if there were any changes in the shape of the gas adsorption isotherms or the level of gas uptake on the particles at higher pressures, this information would not be captured by the Freundlich isotherm model we have used. That is, the calculated isotherms in Fig. 12 were based on gas adsorption data on the polymers obtained at pressures only as high as 1 atm, so the predictions represent a considerable extrapolation of the gas adsorption behavior on the particles. It is not known how much this extrapolation might contribute to the error in the calculated sorption isotherms.

To determine how much of the increase in permeability with increasing particle content was due to changes in gas solubility and how much was due to changes in diffusivity, the sorption isotherms in Fig. 10 were used to estimate gas solubility values according to Eq. (5). The resulting solubility coefficients are presented in Fig. 13. Gas solubility in the nanocomposites is, at most, slightly higher than that in the unfilled PTMSP, so the effect of the particles on gas solubility does not account for the increase in permeability values at increasing particle loadings. Therefore, increases in gas diffusion coefficients with increasing particle loading must account for the high permeability in MgO filled PTMSP.

Gas diffusion coefficients were determined according to Eq. (4), using permeability data at $\Delta p = 3.4$ atm. Gas diffusion coefficients in unfilled PTMSP from this study are within the range

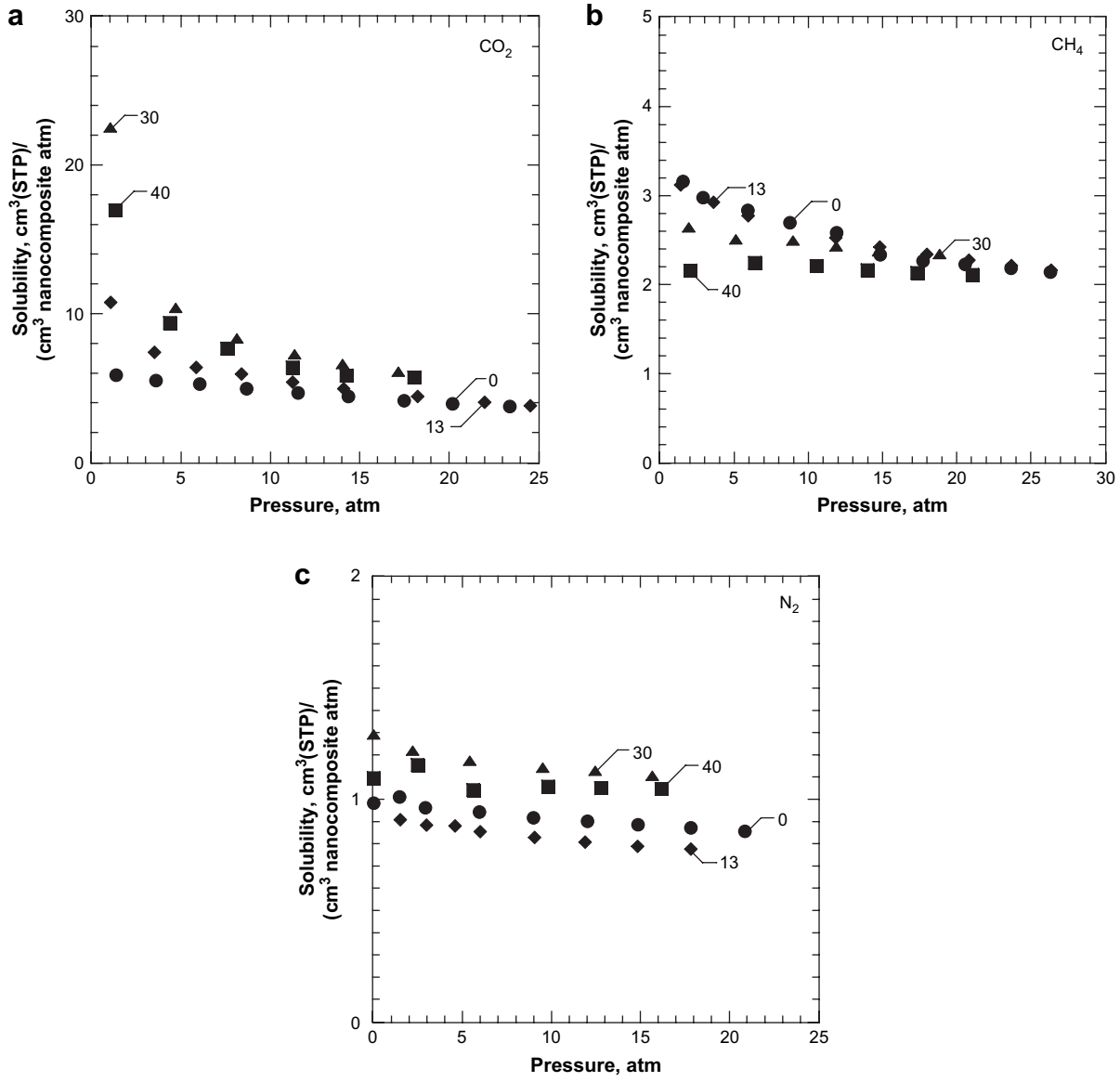

Fig. 13. Solubility coefficients at $p = 4.4$ atm for (a) CO_2, (b) CH_4, and (c) N_2 in PTMSP nanocomposites containing 0 (●), 13 (◆), 30 (▲), and 40 (■) nominal volume percent MgO at 35 °C. Solubility coefficients were calculated using Eq. (5).

of values reported in the literature, as shown in Table 3 [52–54]. The rather large range of gas diffusion coefficients for unfilled PTMSP has been attributed to the sensitivity of gas permeability and diffusivity in PTMSP to film preparation protocols [24].

Fig. 14 presents the influence of particle concentration on gas diffusion coefficients in the nanocomposites relative to their values in pure PTMSP. The diffusion coefficients increase with increasing particle loadings. Interestingly, gas diffusion coefficients exhibit a similar trend when compared to the nanocomposite void content, as shown in Fig. 15.

The overwhelming source of the increase in permeability with increasing particle loading comes from the increase in diffusion coefficients, which is attributed to the void space in the nanocomposites. For example, in PTMSP containing 40 nominal volume percent MgO, the increase in CO_2 diffusion coefficients accounts for approximately 75 percent of

Table 3
Pure gas diffusion coefficients in unfilled PTMSP

Penetrant	Diffusion coefficient × 10^6, cm^2/s				
	This work, 35 °C	Srinivasan et al. [53], 25 °C	Ichiraku et al. [52], 30 °C	Merkel et al. [29], 35 °C	Raharjo et al. [54], 35 °C
CO_2	48 ± 5	30	22	33	–
CH_4	60 ± 6	32	23	36	70
N_2	63 ± 6	36	26	44	–

Error bars were estimated according to the propagation of errors method described by Bevington and Robinson [41].

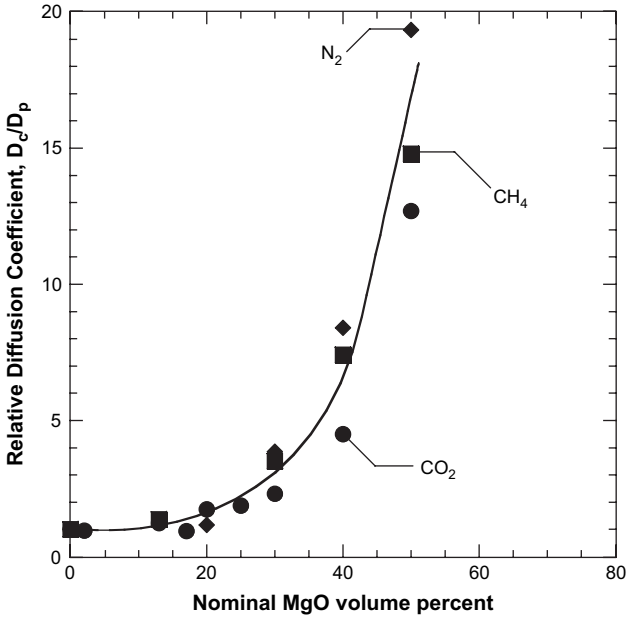

Fig. 14. Relative concentration averaged diffusion coefficients at $\Delta p = 3.4$ atm for CO_2 (●), CH_4 (■), and N_2 (◆) as a function of MgO particle loading in PTMSP. D_c is the concentration averaged diffusion coefficient in the nanocomposite and D_p is the concentration averaged diffusion coefficient in the unfilled polymer. Concentration averaged diffusion coefficients were calculated from Eqs. (4) and (5), where P was obtained from experimental data at 35 °C, and solubility was linearly interpolated to 4.4 atm. The trend line is drawn to guide the eye.

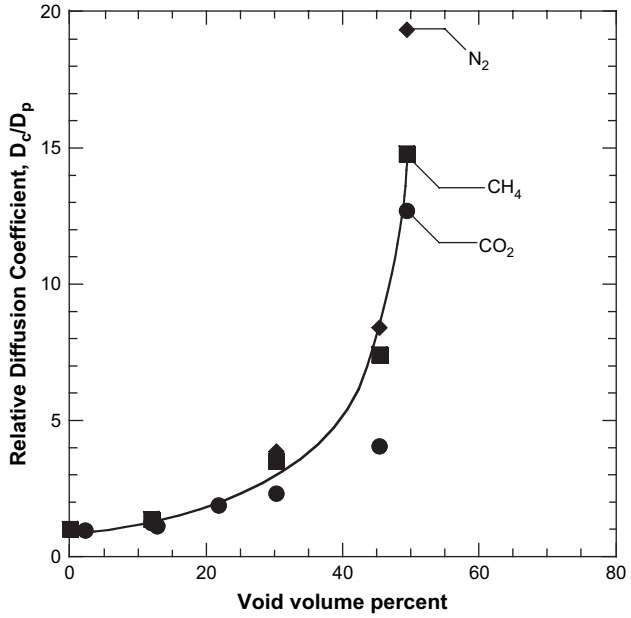

Fig. 15. Relative concentration averaged diffusion coefficients at $\Delta p = 3.4$ atm for CO_2 (●), CH_4 (■), and N_2 (◆) as a function of void volume percent as calculated by Eq. (11). D_c is the concentration averaged diffusion coefficient in the nanocomposite and D_p is the concentration averaged diffusion coefficient in the unfilled polymer. Concentration averaged diffusion coefficients were calculated from Eqs. (4) and (5), where P was obtained from experimental data at 35 °C, and solubility was linearly interpolated to 4.4 atm. The trend line is drawn to guide the eye.

the increase in permeability of CO_2, whereas the solubility behavior only accounts for approximately 25 percent of CO_2 permeability enhancement. Although the exact contributions of diffusivity and solubility to the nanocomposite permeability depend on particle loading and the gas, these results illustrate the relative scale of the contributions. The Bruggeman model correlates the permeability data reasonably well (*cf.*, Fig. 5), because the model is mainly designed to capture the influence of diffusivity on permeability [55], and diffusivity is the main source of permeability enhancement.

4.5. Aging

Gas permeability decreases with time in glassy polymers, in a process commonly referred to as physical aging [24,56]; PTMSP often shows more extensive decreases in permeability over time than other, lower free volume, glassy polymers [57]. However, the dispersion of brookite nanoparticles into PTMSP slowed the rate of permeability reduction with time [23]. In PTMSP films containing 20 nominal volume percent MgO, the CO_2 permeability decreases at approximately the same rate as in unfilled PTMSP, as shown in Fig. 16. However, a film containing 75 volume percent MgO does not exhibit a permeability loss over time. Aging in glassy polymers is associated with polymer chain motion and non-equilibrium excess free volume associated with the polymer [58]. The film containing 75 nominal volume percent MgO is predominantly void space (*cf.*, Fig. 3) and this void space is not necessarily associated with the polymer non-equilibrium free

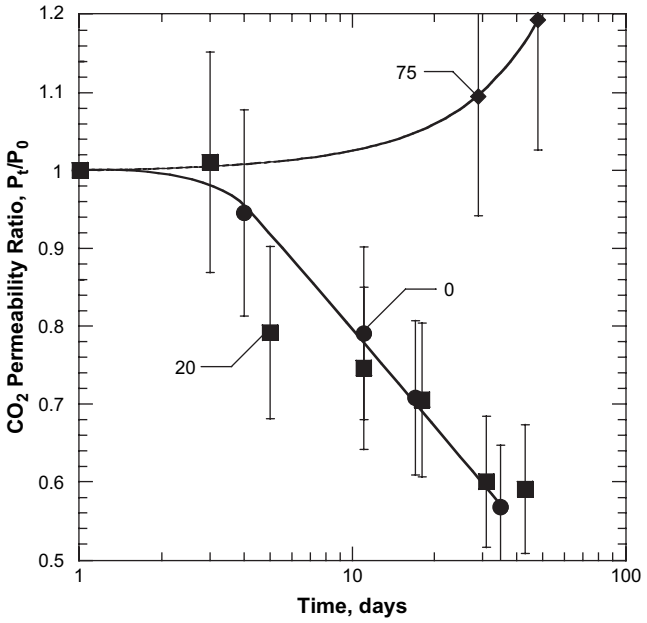

Fig. 16. CO_2 aging ratio (permeability of a sample at time t, P_t, and relative to the permeability at time 0, P_0) at 35 °C and $\Delta p = 3.4$ atm as a function of time for PTMSP containing 0 (●), 20 (■), and 75 (◆) nominal volume percent MgO. Samples were stored in air at room temperature between permeation measurements. Trend lines are drawn to guide the eye. Error bars were estimated from the variance in permeability for multiple experiments using the propagation of errors method described by Bevington and Robinson [41].

volume. Any voids at the particle–polymer interface or in the interparticle spacing might not be influenced by physical aging in the polymer phase, which would account for the permeability stability in PTMSP films containing high concentrations of MgO. It is not clear why permeability in the film containing 75 nominal volume percent MgO increases over time. However, the uncertainty in relative permeability is approximately ±14%, so it is feasible that the permeability in the film containing 75 nominal volume percent MgO is essentially equal to that of a fresh, unaged sample. However, it is also conceivable that a reaction involving exposure of the film to ambient laboratory conditions (*i.e.*, sorption of water, reaction with water, *etc.*) over an extended period of time could occur and the influence of such events on permeability is not known.

5. Conclusions

Based on TEM imaging, MgO nanoparticles dispersed in PTMSP form micron size aggregates. As the nanoparticle concentration increases, void volume and gas permeability increase strongly. The permeability enhancement was due in large part to an increase in gas diffusion coefficients with increasing void space in the nanocomposite. For example, CO_2 permeability in a sample containing 40 nominal volume percent MgO was 4.5 times higher than that of the unfilled polymer, and 75 percent of this increase was due to an increase in the CO_2 diffusion coefficient. Although both gas permeability and diffusion coefficients increase substantially with particle loading, the nanocomposites used in this study were defect-free. There is a good correlation between void volume and permeability, and the increase in permeability with increasing void volume can be modeled using Bruggeman's model. In this system, the dominant impact of the nanoparticles on permeability is to form voids that do not span the sample, which provides high gas transport rates and results in the polymer controlling, to a large extent, the resulting selectivity. Perhaps the aggregates observed in TEM are the locus of this void volume (*i.e.*, between loosely packed particles) but this hypothesis could not be definitively verified. The pure gas selectivity data suggest a stronger role of flow mechanisms, such as Knudsen flow, at the highest particle loadings, suggesting that at high enough particle contents, pore flow transport mechanisms begin to play a role in the overall transport properties in these materials.

Acknowledgement

We gratefully acknowledge partial support of this work by the U.S. Department of Energy (Grant No. DE-FG03-02ER15362).

Appendix. Supplementary information

Supplementary data associated with this article can be found, in the online version, at doi:10.1016/j.polymer.2008.01.004.

References

[1] Vu DQ, Koros WJ, Miller SJ. Mixed matrix membranes using carbon molecular sieves I. Preparation and experimental results. Journal of Membrane Science 2003;211:311–34.
[2] Merkel TC, Freeman BD, Spontak RJ, He Z, Pinnau I, Meakin P, et al. Ultrapermeable, reverse-selective nanocomposite membranes. Science 2002;296:519–22.
[3] Barsema JN, Balster J, Jordan V, van der Vegt NFA, Wessling M. Functionalized carbon molecular sieve membranes containing Ag-nanoclusters. Journal of Membrane Science 2003;219:47–57.
[4] Jose B, Ryu JH, Kim YJ, Kim H, Kang YS, Lee SD, et al. Effect of plasticizers on the formation of silver nanoparticles in polymer electrolyte membranes for olefin/paraffin separation. Chemistry of Materials 2002;14:2134–9.
[5] De Sitter K, Winberg P, D'Haen J, Dotremont C, Leysen R, Martens JA, et al. Silica filled poly(1-trimethylsilyl-1-propyne) nanocomposite membranes: relation between gas transport and structural characteristics. Journal of Membrane Science 2006;278:83–91.
[6] Koros WJ, Pinnau I. Membrane formation for gas separation processes. In: Paul DR, Yampolskii YP, editors. Polymeric gas separation membranes. Boca Raton: CRC Press; 1994. p. 209–71.
[7] Robeson LM. Correlation of separation factor versus permeability for polymeric membranes. Journal of Membrane Science 1991;62:165–85.
[8] Freeman BD. Basis of permeability/selectivity tradeoff relations in polymeric gas separation membranes. Macromolecules 1999;32:375–80.
[9] Barrer RM, Barrie JA, Rogers MG. Heterogeneous membranes: diffusion in filled rubber. Journal of Polymer Science, Part A: Polymer Chemistry 1963;1:2565–86.
[10] Bouma RHB, Checchetti A, Chidichimo G, Drioli E. Permeation through a heterogeneous membrane: the effect of the dispersed phase. Journal of Membrane Science 1997;128:141–9.
[11] Vu DQ, Koros WJ, Miller SJ. Mixed matrix membranes using carbon molecular sieves II. Modeling permeation behavior. Journal of Membrane Science 2003;211:335–48.
[12] He Z, Pinnau I, Morisato A. Nanostructured poly(4-methyl-2-pentyne)/silica hybrid membranes for gas separation. Desalination 2002;146:11–5.
[13] Merkel TC, Freeman BD, Spontak RJ, He Z, Pinnau I, Meakin P, et al. Sorption, transport, and structural evidence for enhanced free volume in poly(4-methyl-2-pentyne)/fumed silica nanocomposite membranes. Chemistry of Materials 2003;15:109–23.
[14] Kim JH, Min BR, Hoon SK, Won J, Kang YS. Facilitated transport of ethylene across polymer membranes containing silver salt: effect of BF_4 on photoreduction of silver ions. Journal of Membrane Science 2003;212:283–8.
[15] Lape NK, Nuxoll EE, Cussler EL. Polydisperse flakes in barrier films. Journal of Membrane Science 2004;236:29–37.
[16] Ghosal K, Freeman BD. Gas separation using polymer membranes: an overview. Polymers for Advanced Technology 1994;5:673–97.
[17] Kang YS, Kang SW, Kim H, Kim JH, Won J, Kim CK, et al. Interaction with olefins of the partially polarized surface of silver nanoparticles activated by *p*-benzoquinone and its implications for facilitated olefin transport. Advanced Materials 2007;19:475–9.
[18] Paul DR, Kemp DR. Diffusion time lag in polymer membranes containing adsorptive fillers. Journal of Polymer Science, Polymer Symposia 1973;41:79–93.
[19] Matteucci S, Yampol'skii YP, Freeman BD, Pinnau I. Transport of gases and vapors in glassy and rubbery polymers. In: Yampol'skii YP, Freeman BD, Pinnau I, editors. Materials science of membranes for gas and vapor separations. London: John Wiley and Sons; 2006. p. 1–48.
[20] Wijmans JG, Baker RW. The solution-diffusion model: a unified approach to membrane permeation. In: Yampol'skii YP, Pinnau I, Freeman BD, editors. Materials science of membranes for gas and vapor separation. London: John Wiley and Sons; 2006. p. 159–90.
[21] Merkel TC, He Z, Pinnau I, Freeman BD, Meakin P, Hill AJ. Sorption and transport in poly(2,2-bis(trifluoromethyl)-4,5-difluoro-1,3-dioxole-

co-tetrafluoroethylene) containing nanoscale fumed silica. Macromolecules 2003;36:8406–14.
[22] Takahashi S, Paul DR. Gas permeation in poly(ether imide) nanocomposite membranes based on surface-treated silica. Part 1: without chemical coupling to matrix. Polymer 2006;47:7519–34.
[23] Matteucci S, Kusuma V, Sanders D, Swinnea S, Freeman BD. Gas transport in TiO_2 nanoparticle filled poly(1-trimethylsilyl-1-propyne). Journal of Membrane Science 2008;307:196–217.
[24] Nagai K, Masuda T, Nakagawa T, Freeman BD, Pinnau I. Poly[1-(trimethylsilyl)-1-propyne] and related polymers: synthesis, properties and functions. Progress in Polymer Science 2001;26:721–98.
[25] Matteucci S, van Wagner E, Swinnea S, Freeman BD, Sakaguchi T, Masuda T. Desilylation of substituted polyacetylenes in the presence of nanoparticles. Macromolecules 2007;40:3337–47.
[26] Tanem BS. Sample preparation and AFM analysis of heterophase polypropylene system. Polymer 2003;44:4283–91.
[27] Lin H, Freeman BD. Gas solubility, diffusivity and permeability in poly(ethylene oxide). Journal of Membrane Science 2004;239:105–17.
[28] Stern SA, Gareis PJ, Sinclair TF, Mohr PH. Performance of a versatile variable-volume permeability cell. Comparison of gas permeability measurements by the variable-volume and variable-pressure methods. Journal of Applied Polymer Science 1963;7:2035–51.
[29] Merkel TC, Bondar V, Nagai K, Freeman BD. Sorption and transport of hydrocarbon and perfluorocarbon gases in poly(1-trimethylsilyl-1-propyne). Journal of Polymer Science, Part B: Polymer Physics 2000;38:273–96.
[30] McDowell CC, Coker DT, Freeman BD. An automated spring balance for kinetic gravimetric sorption of gases and vapors in polymers. Review of Scientific Instruments 1998;69:2510–3.
[31] Bondar VI, Freeman BD, Pinnau I. Gas sorption and characterization of poly(ether-*b*-amide) segmented block copolymers. Journal of Polymer Science, Part B: Polymer Physics 1999;37:2463–75.
[32] Wiederhorn S, Fields R, Low S, Bahng G, Wehrstedt A, Hahn J, et al. Mechanical properties. In: Czichos H, Smith LE, Saito T, editors. Handbook of materials measurement methods. Springer; 2005. p. 283–397.
[33] Qiu J, Zheng J-M, Peinemann K-V. Gas transport properties in a novel poly(trimethylsilylpropyne) composite membrane with nanosized organic filler trimethylsilylglucose. Macromolecules 2006;39:4093–100.
[34] Matteucci S, Raharjo R, Kusuma VA, Swinnea S, Freeman BD. Permeability, solubility and diffusion coefficients in 1,2-polybutadiene containing magnesium oxide. Macromolecules, in preparation.
[35] Mahajan R, Koros WJ. Factors controlling successful formation of mixed-matrix gas separation materials. Industrial and Engineering Chemistry Research 2000;39:2692–6.
[36] Mahajan R, Koros WJ. Mixed matrix membrane materials with glassy polymers. Part 2. Polymer Engineering and Science 2002;42:1432–41.
[37] van der Marck SC. Percolation thresholds of the duals of the face-centered-cubic, hexagonal-close-packed, and diamond lattices. Physical Review E 1997;55:6593–7.
[38] Pinnau I, Toy LG. Transport of organic vapors through poly(1-trimethylsilyl-1-propyne). Journal of Membrane Science 1996;116:199–209.
[39] Merkel TC, He Z, Pinnau I, Freeman BD, Hill AJ, Meakin P. Effect of nanoparticles on gas sorption and transport in poly(1-trimethylsilyl-1-propyne). Macromolecules 2003;36:6844–55.
[40] Bird RB, Stewart WE, Lightfoot EL. Transport phenomena. 2nd ed. New York: John Wiley and Sons; 2002.
[41] Bevington PR, Robinson DK. Data reduction and error analysis for the physical sciences. 3rd ed. New York: McGraw-Hill, Inc.; 2003.
[43] Kesting RE, Fritzsche AK. Polymer gas separation membranes. New York: John Wiley and Sons; 1993.
[44] Eletskii AV. Viscosity. In: Grigoriev IS, Meilikhov EZ, editors. Handbook of physical quantities. New York: CRC Press; 1997. p. 451–64.
[45] Breck DW. Zeolite molecular sieves: structure, chemistry, and use. New York: John Wiley and Sons; 1974. 593–724.
[46] Do DD. Adsorption analysis: equilibria and kinetics. In: Series on chemical engineering, vol. 2. London: Imperial College Press; 1998.
[47] Koros WJ, Chan AH, Paul DR. Sorption and transport of various gases in polycarbonate. Journal of Membrane Science 1977;2:165–90.
[48] Paul DR. Gas sorption and transport in glassy polymers. Berichte der Bunsen-Gesellschaft-Physical Chemistry Chemical Physics 1979;83:294–302.
[49] Matteucci S, Kusuma VA, Swinnea S, Freeman BD. Light gas permeability, solubility and diffusion in 1,2-polybutadiene containing brookite nanoparticles. Polymer, in preparation.
[50] Mekhemer GAH, Halaway SA, Mohamed MA, Zaki MI. Qualitative and quantitative assessments of acid and base sites exposed on polycrystalline MgO surfaces: thermogravimetric, calorimetric, and in-situ FTIR spectroscopy study combination. Journal of Physical Chemistry B 2004;108:13379–86.
[51] Stark JV, Park DG, Lagadic I, Klabunde KJ. Nanoscale metal oxide particles/clusters as chemical reagents. Unique surface chemistry on magnesium oxide as shown by enhanced adsorption of acid gases (sulfur dioxide and carbon dioxide) and pressure dependence. Chemistry of Materials 1996;8:1904–12.
[52] Ichiraku Y, Stern SA, Nakagawa T. An investigation of the high gas permeability of poly(1-trimethylsilyl-1-propyne). Journal of Membrane Science 1987;34:5–18.
[53] Srinivasan R, Auvil SR, Burban PM. Elucidating the mechanism(s) of gas transport in poly[1-(trimethylsilyl)-1-propyne] (PTMSP) membranes. Journal of Membrane Science 1994;86:67–86.
[54] Raharjo RD, Freeman BD, Paul DR, Sanders ES. Pure and mixed gas CH_4 and n-C_4H_{10} permeability and diffusivity in poly(1-trimethylsilylpropyne). Polymer 2007;48:7329–44.
[55] Barrer RM. Diffusion and permeation in heterogeneous media. In: Crank J, Park GS, editors. Diffusion in polymers. New York: Academic Press; 1968. p. 165–219.
[56] McCaig MS, Paul DR. Effect of film thickness on the changes in gas permeability of a glassy polyarylate due to physical aging. Part I. Experimental observations. Polymer 2000;41:629–37.
[57] Nagai K, Nakagawa T. Effects of aging on the gas permeability and solubility in poly(1-trimethylsilyl-1-propyne) membranes synthesized with various catalysts. Journal of Membrane Science 1995;105:261–72.
[58] Pfromm PH. The impact of physical aging of amorphous glassy polymers on gas separation membranes. In: Yampol'skii YP, Pinnau I, Freeman BD, editors. Materials science of membranes for gas and vapor separation. London: John Wiley and Sons; 2006. p. 293–306.